Journal of Biomedical Optics

BiomedicalOptics.SPIEDigitalLibrary.org

Intracellular imaging of docosanol in living cells by coherent anti-Stokes Raman scattering microscopy

Sixian You
Yuan Liu
Zane Arp
Youbo Zhao
Eric J. Chaney
Marina Marjanovic
Stephen A. Boppart

SPIE.

Sixian You, Yuan Liu, Zane Arp, Youbo Zhao, Eric J. Chaney, Marina Marjanovic, Stephen A. Boppart, "Intracellular imaging of docosanol in living cells by coherent anti-Stokes Raman scattering microscopy," *J. Biomed. Opt.* **22**(7), 070502 (2017), doi: 10.1117/1.JBO.22.7.070502.

Intracellular imaging of docosanol in living cells by coherent anti-Stokes Raman scattering microscopy

Sixian You,[a,b] Yuan Liu,[a,b] Zane Arp,[c] Youbo Zhao,[a] Eric J. Chaney,[a] Marina Marjanovic,[a,b] and Stephen A. Boppart[a,b,d,e,*]

[a]University of Illinois at Urbana-Champaign, Beckman Institute for Advanced Science and Technology, Urbana, Illinois, United States
[b]University of Illinois at Urbana-Champaign, Department of Bioengineering, Urbana, Illinois, United States
[c]GlaxoSmithKline, King of Prussia, Pennsylvania, United States
[d]University of Illinois at Urbana-Champaign, Department of Electrical and Computer Engineering, Urbana, Illinois, United States
[e]University of Illinois at Urbana-Champaign, Department of Internal Medicine, Urbana, Illinois, United States

Abstract. Docosanol is an over-the-counter topical agent that has proved to be one of the most effective therapies for treating herpes simplex labialis. However, the mechanism by which docosanol suppresses lesion formation remains poorly understood. To elucidate its mechanism of action, we investigated the uptake of docosanol in living cells using coherent anti-Stokes Raman scattering microscopy. Based on direct visualization of the deuterated docosanol, we observed highly concentrated docosanol inside living cells 24 h after drug treatment. In addition, different spatial patterns of drug accumulation were observed in different cell lines. In keratinocytes, which are the targeted cells of docosanol, the drug molecules appeared to be docking at the periphery of the cell membrane. In contrast, the drug molecules in fibroblasts appeared to accumulate in densely packed punctate regions throughout the cytoplasm. These results suggest that this molecular imaging approach is suitable for the longitudinal tracking of drug molecules in living cells to identify cell-specific trafficking and may also have implications for elucidating the mechanism by which docosanol suppresses lesion formation. [DOI: 10.1117/1.JBO.22.7.070502]

Keywords: intracellular imaging; docosanol; herpes simplex virus-1; coherent Raman imaging.

Paper 170285LR received May 1, 2017; accepted for publication Jul. 5, 2017; published online Jul. 25, 2017.

1 Introduction

Recurrent herpes simplex labialis (HSL), also referred to as cold sores or fever blisters by the general population, is a common infection caused by herpes simplex virus type 1 (HSV-1), affecting at least 20% of the adult population in the United States.[1,2] HSV-1 has been known to be incurable and persistent once the host is infected.[3] After the primary infection, the virus establishes latency within the trigeminal ganglion and evades immune surveillance before being reactivated by environmental triggers, such as emotional stress, illness, sunlight, and menstruation.[4] Although HSL is self-limiting and mostly nonfatal, there is a great demand for better treatment due to the discomfort and negative social consequences associated with this disease.[5–7]

Current antiviral agents for HSV infection aim to attenuate the clinical course of the disease via the inhibition of viral replication.[3] One of the most successful agents is acyclovir (1977), the first effective drug for the treatment of HSV infections.[8] Acyclovir is a type of nucleoside analogue that targets viral DNA polymerase and, thus, blocks viral replication processes.[9] Despite its effectiveness in altering viral DNA activity in the trials, acyclovir and its related drugs have a risk of being toxic, mutagenic, and inducing drug-resistant strains after long-term use.[10] A new agent, docosanol with mechanisms of action was proposed in 1988 and is now an over-the-counter topical agent that has proved to be one of the most effective therapies for treating HSL. Docosanol is a 22-carbon-long, aliphatic, and straight-chain saturated alcohol that inhibits a variety of lipid-enveloped viruses including HSV-1.[5,10,11] Instead of directly targeting viral DNA replication, docosanol interferes with the fusion between the host cell membrane and the viral envelope and, thus, inhibits viral entry and subsequent replication.[3,5,10] This new mechanism of action is likely responsible for the higher threshold of toxicity and the lower drug resistance exhibited during docosanol treatments.[11,12] Nevertheless, the precise mechanism of its action remains unknown and has not yet been empirically demonstrated with intracellular imaging, which limits further development of more effective treatments for HSV-1.[4,11]

Fluorescence assays have been performed on fixed cells to characterize docosanol treatment.[10] However, direct visualization of docosanol interference in living cells, despite its importance for understanding the precise mechanism of the treatment, has not yet been shown. Recent studies show that vibrational imaging can be a powerful tool for tracing drugs in living cells. Compared with other available imaging techniques, such as magnetic resonance imaging, positron emission tomography, and fluorescence imaging, vibrational imaging is more suitable for visualizing docosanol in living cells due to its unique advantages of spatial–chemical specificity to small molecules, subcellular resolution, and minimal physiological perturbation.[13–15] Here, we report that by using coherent Raman scattering microscopy, we are able to visualize the intracellular distribution of deuterated docosanol in living cells. Coherent Raman scattering microscopy is a label-free, high-resolution, vibrational imaging technique that has proven capable of acquiring spatiotemporal and compositional information from biological systems within minutes.[16–18] Compared with spontaneous Raman scattering, the process of coherent Raman scattering is significantly more efficient due to the resonant amplification in the nonlinear interaction, which enables high-speed imaging with high chemical specificity and subcellular spatial resolution.[19–21] These properties of coherent Raman scattering microscopy make it ideal for investigating the unique mechanism by which docosanol interacts with cells.

*Address all correspondence to: Stephen A. Boppart, E-mail: boppart@illinois.edu

1083-3668/2017/$25.00 © 2017 SPIE

The objective of this study, therefore, is to visualize the intracellular distribution of docosanol inside living cells using coherent Raman scattering microscopy. To reduce the operating complexity and bulkiness usually associated with coherent Raman scattering microscopy systems, a custom-made fiber source-based coherent anti-Stokes Raman scattering (CARS) imaging system was used.[22] Deuterated docosanol was designed to shift characteristic Raman bands from C—H stretching modes (2800 to 3100 cm^{-1}) to C—D stretching modes (2000 to 2300 cm^{-1}), which is known to be in the cellular silent region.[13] Highly concentrated docosanol was found inside living cells 24 h after drug treatment. Furthermore, the subcellular behavior of docosanol was shown to vary with different cell lines. In keratinocytes, which are the targeted cell line of docosanol, the drug molecules appeared to be docking at the interior of the cell membrane. In contrast, the drug molecules in fibroblasts appeared to accumulate in densely packed punctate regions throughout the cytoplasm. These results indicate that this molecular imaging strategy has high potential for elucidating the mechanism by which docosanol interacts with specific cell types to suppress lesion formation in the skin.

2 Materials and Methods

2.1 *Materials*

The deuterated docosanol was obtained from GlaxoSmithKline. The powder form of the drug was used to acquire a standard spectrum using spontaneous Raman scattering and CARS spectroscopy. Dimethyl sulfoxide (DMSO), the solvent for the drug, was purchased from Sigma-Aldrich.

2.2 *Cell Culture*

Both human dermal fibroblasts and human epidermal keratinocytes were purchased from ZenBio, Inc. Fibroblasts were cultured in dermal fibroblast culture medium (DF-1, ZenBio). Keratinocytes were cultured in adult keratinocyte growth medium (KM-2, ZenBio). Both cell cultures were grown in cell culture flasks at 37°C with 5% CO_2 and passaged onto Petri dishes two days before imaging.

2.3 *Coherent Anti-Stokes Raman Scattering Imaging*

A previously described, custom-made, fiber supercontinuum-based system (Fig. 1) was used for CARS imaging in the silent spectral region (2000 to 2500 cm^{-1}) of docosanol in living cells.[22,23] Briefly, pulses (1041 nm, 220 fs, 80 MHz) from a Yb:KYM laser (femtoTRAIN IC model-Z, High Q Laser) were sent into a 21-cm long photonic crystal fiber (NL-1050-NEG-PM-FUD, NKT Photonics) to generate a widely coherent supercontinuum from 780 to 1320 nm. The supercontinuum output was separated into the pump beam (780 to 880 nm) and the Stokes beam (900 to 1320 nm) by a dichroic mirror (DMLP900, Thorlabs). The targeted wave number of this spectral-focusing-based CARS imaging system was determined by the temporal delay between the pump and the Stokes beam and was controlled by a motorized stage in the path of the Stokes beam. The two beams were then recombined by a second dichroic mirror, sent into a commercial microscope (BX61WI, Olympus), and focused by a superapochromat objective (UPLSAPO 60XW/IF, N.A. 1.20, Olympus). The optical power at the sample was 8 mW for the pump beam and 20 mW for the Stokes beam. The forward-directed CARS signals were collected by a second objective (LUMPlanFl/IR 60XW, N.A. 0.9, Olympus). The mapping relationship between the temporal delay and the true wave number was determined and calibrated using the spectral peaks of acetonitrile and the drug powder. The spectral resolution was ~20 to 30 cm^{-1}. The pixel dwelling time in each CARS image was 1 ms.

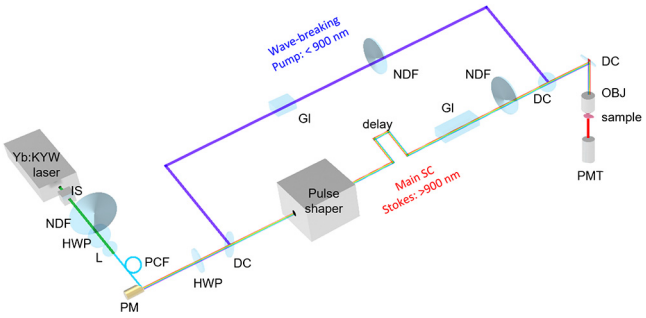

Fig. 1 A schematic diagram of the CARS imaging system. DC, dichroic mirror; FW, filter wheel; GI, glass; HWP, half-wave plate; IS, isolator; KYW, potassium yttrium tungstate; L, lens; NDF, neutral density filter; OBJ, objective; PCF, photonic crystal fiber; PM, parabolic mirror; PMT, photomultiplier tube; and Yb, ytterbium.

2.4 *Coherent Anti-Stokes Raman Scattering Imaging of Drug-Treated Cells*

The deuterated drug was dissolved in DMSO at the concentration of 10 mM. For the drug treatment studies, 30 μL of the drug solution was added to a cell culture dish along with 3 mL of cell culture media (dermal fibroblast culture medium and adult keratinocyte growth medium for fibroblast and keratinocyte, respectively), resulting in a final concentration of the drug at ~100 μM. After 24 h of incubation, the cell media was replaced with fresh media and the cells were immediately imaged.

3 Results and Discussion

3.1 *Spontaneous and Coherent Raman Spectroscopy of the Drug Molecules*

The spontaneous Raman spectrum of the drug molecule was obtained using a commercial Raman microscope (Horiba LabRAM HR 3D, Horiba). As shown in Fig. 2(a), several characteristic C—D vibrational peaks appear around 2100 cm^{-1} in the cellular silent region (2000 to 2300 cm^{-1}), which is attributed to the replacement of multiple C—H bonds with C—D bonds in the deuterated drug.[24,25] In particular, the unique strong peak around 2100 cm^{-1} was used as the spectral region of interest in this study. To examine the possible distortion of the CARS spectrum, the drug molecule was measured by CARS spectroscopy in the silent region to compare with the spontaneous Raman spectrum [Fig. 2(b)]. The high degree of similarity between these two spectra demonstrated the feasibility of this experiment. The noticeably reduced spectral resolution can be attributed to the limitation of the spectral-focusing-based CARS setup.

3.2 *Drug Accumulation in Fibroblasts*

Drug-treated fibroblasts were imaged at two frequencies, 2100 cm^{-1} for the resonant frequency and 2250 cm^{-1} for the

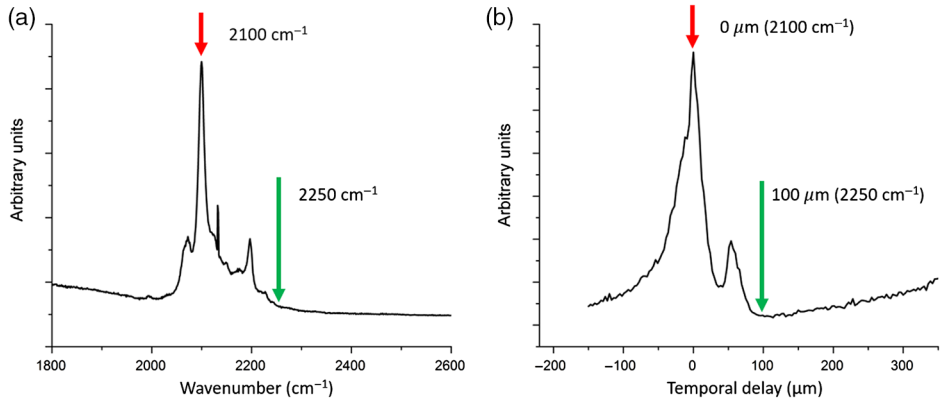

Fig. 2 Drug vibrational spectrum by (a) spontaneous Raman scattering spectroscopy and (b) CARS spectroscopy. The temporal delay of 0 μm in the CARS spectrum corresponds to the wave number of 2100 cm^{-1} in the spontaneous Raman spectrum, which was used as the drug-resonant peak in this study. The temporal delay of 100 μm in the CARS spectrum corresponds to the wave number of 2250 cm^{-1} in the spontaneous Raman spectrum, which was used as the nonresonant region in this study.

nonresonant frequency. Figure 3 shows the representative (a) drug-resonant CARS image, (b) the drug nonresonant CARS image, and (c) the composite image. Bright, densely packed punctate regions were observed inside the cells. Representative CARS spectra collected from pixels of interest within the CARS image are shown in Fig. 3(d). Compared with the spectrum acquired from the background of the cell body, the spectrum of the bright punctate regions has a unique, sharp, and strong peak at 2100 cm^{-1}. Furthermore, the spectra representing the bright regions strongly resemble the drug spectra acquired from the spontaneous Raman scattering and CARS spectroscopy (Fig. 2). Interestingly, the drug areas appear much darker than the surroundings in the nonresonant image [Fig. 3(b)]. This can be explained by the lack of water component in the highly concentrated drug area, which results in the sharp decrease of nonresonant CARS signal compared with the nondrug areas. These observations support the hypothesis that the punctate regions within the fibroblasts are indeed the result of highly concentrated drug.

3.3 *Drug Accumulation in Keratinocytes*

Following the demonstration of drug accumulation within living fibroblasts, a similar study was conducted with human epidermal keratinocytes, which are the targeted cells for docosanol treatment. Figure 4 shows (a) the drug-resonant CARS image, (b) the nonresonant CARS image, and (c) the composite image of the two frequencies. Interestingly, a bright ring was observed around the periphery of the keratinocytes, unlike the pattern of punctate regions within the fibroblasts. The CARS spectra, shown in Fig. 4(d), indicate that the bright ring is the result of drug accumulation in the keratinocytes. This observation is highly intriguing because this particular distribution pattern resonates with the predominant mechanism of action for docosanol, which is reported to be an interaction with the cell membrane to inhibit the fusion between the cell plasma membrane and the HSV envelope.[10,11] Further studies are needed to investigate whether this distribution of docosanol within the cell membrane is directly responsible for its mechanism of inhibiting viral entry.

In summary, our study visualizes the intracellular distribution of docosanol in fibroblasts and keratinocytes, and reveals cell-specific distribution patterns that may indicate specific mechanisms of drug action and, thus, have important therapeutic implications. These results suggest that docosanol docking at the periphery of keratinocytes might be one of the earlier steps for the inhibition of fusion at the plasma membrane during docosanol treatment. However, the precise mechanism of action

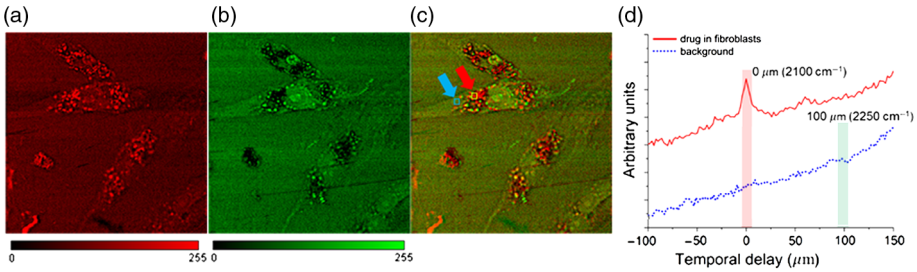

Fig. 3 Hyperspectral CARS imaging shows the accumulation of docosanol in living fibroblasts. Representative CARS image at (a) 2100 cm^{-1} and at (b) 2250 cm^{-1} of drug-treated living fibroblasts. (c) Spatial overlap of the drug-resonant CARS image (green) and the drug-nonresonant image (red). In the resulting composite image, the drug-resonant regions appear red, whereas the nonresonant regions appear yellow. (d) CARS spectra of the bright regions in the cell [red line, corresponding to the red arrow (right arrow)/small yellow box in (c)] and the cell body background [blue line, corresponding to the blue arrow (left arrow)/small blue box in (c)]. Image field of view: 128 × 128 μm^2.

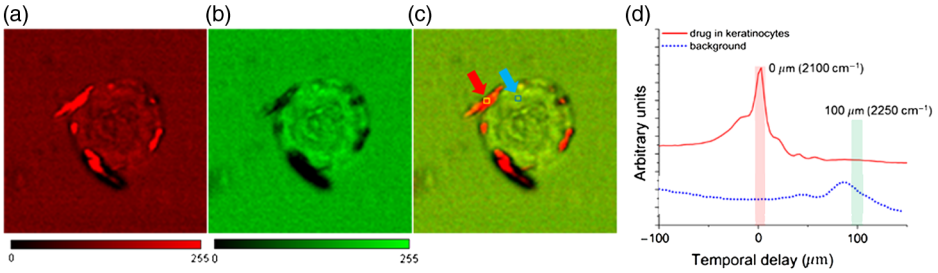

Fig. 4 Hyperspectral CARS imaging shows the accumulation of docosanol in the living keratinocyte. Representative CARS image at (a) 2100 cm^{-1} and at (b) 2250 cm^{-1} of drug-treated living keratinocytes. (c) Spatial overlap of the drug-resonant CARS image (green) and the drug-nonresonant image (red). In the resulting composite image, drug-resonant regions appear red whereas the nonresonant regions appear yellow. (d) CARS spectra of the bright pixels in the cell [red line, corresponding to the red arrow (left arrow)/small yellow box in (c)] and the cell body background [blue line, corresponding to the blue arrow (right arrow)/small blue box in (c)]. Image field of view: 50×50 μm^2.

for docosanol interference remains unclear. To fully understand the process of docosanol interference, more in-depth experiments on infected and subsequently treated keratinocytes will be essential for future studies. We wish to emphasize that the goal of this study is to present initial results demonstrating how a CARS imaging-based method can be used to characterize and observe the intracellular behavior of docosanol in living cells. The investigation model as well as the preliminary results presented in this study demonstrate the potential impact of the proposed methodology on improving the understanding of docosanol treatment.

Disclosures

The authors declare no competing financial interests.

Acknowledgments

The authors would like to thank Darold Spillman and Joanne Li for their assistance with technology support, and Cathy Simmons for assistance with cell culture and compound supplies. This research was supported by a sponsored research agreement from GlaxoSmithKline. Additional information can be found at http://biophotonics.illinois.edu.

References

1. H. Rahimi et al., "Effectiveness of antiviral agents for the prevention of recurrent herpes labialis: a systematic review and meta-analysis," *Oral Surg. Oral Med. Oral Pathol. Oral Radiol.* **113**(5), 618–627 (2012).
2. C. M. Hull et al., "Early treatment of cold sores with topical ME-609 decreases the frequency of ulcerative lesions: a randomized, double-blind, placebo-controlled, patient-initiated clinical trial," *J. Am. Acad. Dermatol.* **64**(4), 696.e1–696.e11 (2011).
3. M. Fatahzadeh and R. A. Schwartz, "Human herpes simplex virus infections: epidemiology, pathogenesis, symptomatology, diagnosis, and management," *J. Am. Acad. Dermatol.* **57**(5), 737–763 (2007).
4. S. Bin Woo and S. J. Challacombe, "Management of recurrent oral herpes simplex infections," *Oral Surg. Oral Med. Oral Pathol. Oral Radiol. Endodontol.* **103**(Suppl.), S12.e1–S12.e18 (2007).
5. S. L. Sacks et al., "Clinical efficacy of topical docosanol 10% cream for herpes simplex labialis: a multicenter, randomized, placebo-controlled trial," *J. Am. Acad. Dermatol.* **45**(2), 222–230 (2001).
6. S. L. Spruance et al., "Single-dose, patient-initiated famciclovir: a randomized, double-blind, placebo-controlled trial for episodic treatment of herpes labialis," *J. Am. Acad. Dermatol.* **55**(1), 47–53 (2006).
7. C. Cernik, K. Gallina, and R. T. Brodell, "The treatment of herpes simplex infections," *Arch. Intern. Med.* **168**(11), 1137–1144 (2008).
8. G. Kleymann, "Novel agents and strategies to treat herpes simplex virus infections," *Expert Opin. Invest. Drugs* **12**(2), 165–183 (2003).
9. Y. Jiang et al., "New strategies against drug resistance to herpes simplex virus," *Int. J. Oral Sci.* **8**(1), 1–6 (2016).
10. L. E. Pope et al., "The anti-herpes simplex virus activity of n-docosanol includes inhibition of the viral entry process," *Antiviral Res.* **40**(1–2), 85–94 (1998).
11. D. H. Katz et al., "Antiviral activity of 1-docosanol, an inhibitor of lipid-enveloped viruses including herpes simplex," *Proc. Natl. Acad. Sci. U. S. A.* **88**(23), 10825–10829 (1991).
12. M. Suzuki, T. Okuda, and K. Shiraki, "Synergistic antiviral activity of acyclovir and vidarabine against herpes simplex virus types 1 and 2 and varicella-zoster virus," *Antiviral Res.* **72**(2), 157–161 (2006).
13. A. F. Palonpon, M. Sodeoka, and K. Fujita, "Molecular imaging of live cells by Raman microscopy," *Curr. Opin. Chem. Biol.* **17**(4), 708–715 (2013).
14. G. Bergner et al., "Quantitative detection of C-deuterated drugs by CARS microscopy and Raman microspectroscopy," *Analyst* **136**(18), 3686 (2011).
15. B. G. Saar et al., "Imaging drug delivery to skin with stimulated Raman scattering microscopy," *Mol. Pharm.* **8**(3), 969–975 (2011).
16. J. Cheng and X. S. Xie, "Coherent anti-Stokes Raman scattering microscopy: instrumentation, theory, and applications," *J. Phys. Chem. B* **108**(3), 827–840 (2004).
17. C. W. Freudiger et al., "Label-free biomedical imaging with high sensitivity by stimulated Raman scattering microscopy," *Science* **322**, 1857–1861 (2008).
18. C. H. Camp, Jr. and M. T. Cicerone, "Chemically sensitive bioimaging with coherent Raman scattering," *Nat. Photonics* **9**(5), 295–305 (2015).
19. D. Fu et al., "Imaging the intracellular distribution of tyrosine kinase inhibitors in living cells with quantitative hyperspectral stimulated Raman scattering," *Nat. Chem.* **6**(7), 614–622 (2014).
20. A. Zumbusch, G. R. Holtom, and X. S. Xie, "Three-dimensional vibrational imaging by coherent anti-Stokes Raman scattering," *Phys. Rev. Lett.* **82**(20), 4142–4145 (1999).
21. D. Fu et al., "Quantitative chemical imaging with multiplex stimulated Raman scattering microscopy," *J. Am. Chem. Soc.* **134**(8), 3623–3626 (2012).
22. H. Tu et al., "Stain-free histopathology by programmable supercontinuum pulses," *Nat. Photonics* **10**(8), 534–540 (2016).
23. Y. Liu et al., "Suppressing short-term polarization noise and related spectral decoherence in all-normal dispersion fiber supercontinuum generation," *J. Lightwave Technol.* **33**(9), 1814–1820 (2015).
24. F. Hu et al., "Live-cell vibrational imaging of choline metabolites by stimulated Raman scattering coupled with isotope-based metabolic labeling," *Analyst* **139**(10), 2312–2317 (2014).
25. A. Alfonso-García et al., "D38-cholesterol as a Raman active probe for imaging intracellular cholesterol storage," *J. Biomed. Opt.* **21**(6), 061003 (2015).